

A Speckle-Enhanced Prism Spectrometer With High Dynamic Range

Ş. Kaan Çetindağ, M. Fatih Toy, Onur Ferhanoglu^{ID}, and Fehmi Çivitci

Abstract—We present a novel spectrometer device offering a wide wavelength range and high resolution. The device builds upon a conventional prism spectrometer; however, an additional scattering medium is introduced to generate a wavelength-dependent speckle pattern on the detector array. Simultaneous use of the prism and the scattering medium allows for both improved resolution and wavelength range. The generated speckle pattern secures a significant improvement in the resolution (up to 100 folds) and dynamic range over a conventional prism spectrometer. With the proposed spectrometer, implemented using a CCD camera, we demonstrate up to 17-pm resolution at 855-nm central wavelength and 756.5-nm wavelength range revealing a dynamic range of ~44 500. The dynamic range could be further improved upon using a detector array having larger area and a scattering medium offering a narrower spectral correlation function. With further development, the proposed device could be useful in a variety of spectroscopy applications, such as deep imaging of retinal layers in optical coherence tomography.

Index Terms—Prism, speckle, spectroscopy.

I. INTRODUCTION

SPECTROSCOPY spans a wide range of applications, including identification of proteins in biology [1], material characterization [2], telecommunication [3], opto-medical imaging (such as Optical Coherence Tomography or shortly OCT) [4], and many others [5]. Thanks to its simplicity and efficacy, spectral-spatial mapping is among the most common techniques in spectroscopy, wherein every wavelength component is mapped to a different spatial position. Conventionally, spectral-spatial mapping is achieved with either a diffraction grating, or a prism. Although diffraction grating spectrometers offer a superior resolution over prism-based spectrometers, they are limited in their wavelength range due to overlapping of diffracted orders [6].

Speckle spectrometry has arisen as a promising alternative, where each wavelength is mapped to a different speckle pattern on the detector array. The reconstruction is performed through

Manuscript received September 11, 2018; revised October 21, 2018; accepted October 30, 2018. Date of publication November 1, 2018; date of current version November 28, 2018. This work was supported by the Scientific and Technological Research Council of Turkey (TUBITAK) under Grant 116F142. (*Corresponding author: Onur Ferhanoglu*.)

Ş. K. Çetindağ, O. Ferhanoglu, and F. Çivitci are with the Department of Electronics and Communication Engineering, Istanbul Technical University, 34469 Istanbul, Turkey (e-mail: ferhanoglu@itu.edu.tr).

M. F. Toy is with the Department of Biomedical Engineering, Istanbul Medipol University, 34810 Istanbul, Turkey.

Color versions of one or more of the figures in this letter are available online at <http://ieeexplore.ieee.org>.

Digital Object Identifier 10.1109/LPT.2018.2879247

first recording the patterns (basis functions) of each wavelength through utilizing a tunable light source, and then finding the weights of the recorded patterns within the captured image for a broad-band source. Yet, implementations of speckle spectrometer are typically fiber-based and showcase a very limited wavelength-range [7], [8].

We present a hybrid prism/speckle spectrometer to simultaneously achieve wide range and high resolution, which we call the speckle-enhanced prism spectrometer (SEPS). SEPS embarks both spectral-spatial mapping and speckle elements. The simultaneous use of the prism and the scattering medium enables both improved resolution (likewise other speckle spectrometers) and high wavelength range (likewise a prism spectrometer). The role of the prism in separating the speckle patterns into different spatial locations is critical in ensuring high speckle contrast, in contrary to speckle spectrometers that dedicate the same detector area for all wavelengths. Although large wavelength range speckle spectrometers were showcased in literature [9] through observing the leakage light from a multimode fiber, SEPS offers higher speckle contrast, once again owing to the distribution of speckle patterns arriving from different wavelengths to different spatial locations on the detector array.

II. SPECTROMETER ARCHITECTURE

Figure 1 illustrates the proposed SEPS architecture. The spectrometer consists of two parts, namely the prism spectrometer for spectral-spatial mapping and the scattering medium that superposes speckle patterns on the spectral-spatial mapping. The light exiting the light source is first collimated, than focused onto the scattering layer with the first cylindrical lens. A 50-μm slit is placed in contact with the scatterer to mitigate an enlarged emission area out of the scatterer, at the expense of light efficiency. A second cylindrical lens once again collimates the light and the rest of the setup is basically a conventional prism spectrometer, where the third cylindrical lens before the detector array forms a focused line per each wavelength component. A typical prism spectrometer in the absence of the scattering layer, exhibits a resolution that is equal to the full-width half-maximum (FWHM) of the formed line ($\Delta\lambda_{\text{prism}}$). Theoretically:

$$\Delta\lambda_{\text{prism}} = \frac{4ln2}{\sigma' Wk} \quad (1)$$

where σ' is the angular dispersion (change of refracted angle at the prism-air interface with respect to wavelength change),

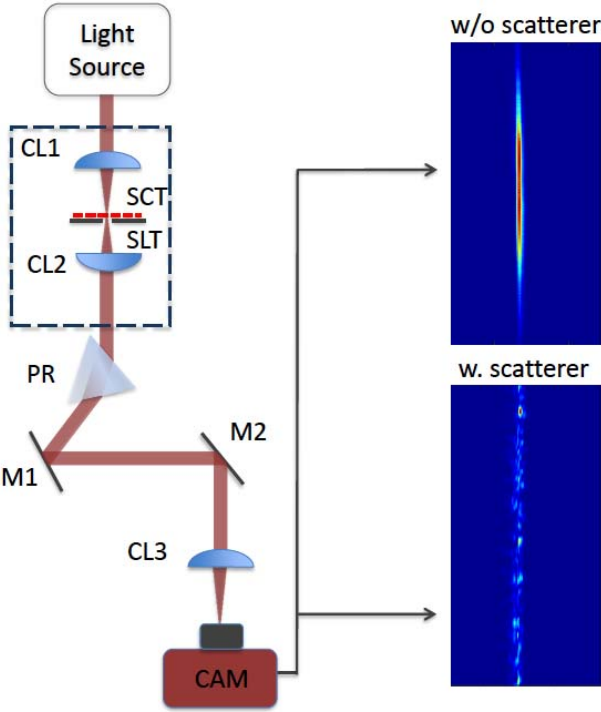


Fig. 1. Speckle-enhanced Prism Spectrometer architecture, illustrating the light source, cylindrical lens pair (CL1, CL2), the scatterer (SCT), the slit (SLT), the prism (PR), two light folding mirrors (M1, M2), final focusing cylindrical lens (CL3), and the CCD camera (CAM). Insets visualize detector images captured for single illumination wavelength with and without the scatterer.

W is the FWHM of the collimated beam arriving at the prism, and k is the wavenumber [10].

Owing to the scattering layer that generates wavelength-dependent speckle patterns, SEPS can resolve with sub-prism resolution, offering a resolution gain factor (K), such that:

$$\Delta\lambda_{SEPS} = \frac{\Delta\lambda_{prism}}{K} \quad (2)$$

The resolution gain factor (K), is proportional with the degree of scattering and should be maximized as long as the system light budget permits. One other advantage of SEPS is improved dynamic range as the wavelength range stays unaltered with respect to a prism spectrometer.

III. SYSTEM CALIBRATION

Prior to the measurement, the system necessitates acquisition of speckle patterns for all wavelengths of interest. Thus, the system should employ a tunable laser (having wavelength sweep steps, $\delta\lambda$, smaller than the system resolution), for calibration. Once speckle images are acquired, system resolution is calculated based on the half-width half-maximum (HWHM) of the spectral correlation function ($C(\Delta\lambda, x)$) [8]:

$$C(\Delta\lambda, x) = \frac{\langle I(\lambda, x)I(\lambda + \Delta\lambda, x) \rangle}{\langle I(\lambda, x) \rangle \langle I(\lambda + \Delta\lambda, x) \rangle} - 1 \quad (3)$$

Where $I(\lambda, x)$ is the intensity recorded at certain wavelength (λ) and position (x), $\Delta\lambda$ refers to the wavelength difference among speckle patterns for which the correlation is calculated and $\langle \cdot \rangle$ is the mean operation. The spectral correlation function is calculated till $\Delta\lambda = \Delta\lambda_{prism}$.

IV. RECONSTRUCTION OF THE SPECTRUM

The spectrum of a broadband source is reconstructed based on the wavelength dependent speckle patterns, such that [8]:

$$I(x) = \int S(\lambda)T(\lambda)d\lambda \quad (4)$$

where $I(x)$ is the intensity of the captured image, $S(\lambda)$ is the speckle pattern acquired for each wavelength and $T(\lambda)$ is the transmission for each wavelength component In matrix form:

$$I = T \cdot S \quad (5)$$

In order to obtain S , the following equation can be utilized;

$$S = T^{-1} \cdot I \quad (6)$$

The inverse of T matrix can be calculated via Moore-Penrose pseudo-inverse method [11], under ideal conditions. On the other hand, in a realistic scenario noise will be imposed on both the speckle images (S) and the total captured image (I), which could result in reconstruction error.

To mitigate reconstruction errors, Singular Value Decomposition (SVD) could be utilized to factorize T [8], such that:

$$T = U \cdot D \cdot V^T \quad (7)$$

Thus;

$$T^{-1} = V \cdot D^{-1} \cdot U^T \quad (8)$$

where D is a diagonal matrix. D^{-1} is also a diagonal matrix composed of the reciprocal of the elements of D . Noise that is superimposed on speckle images results in small-valued diagonal elements in D , which in turn leads to large-valued diagonal elements in D^{-1} . Thus, we implement truncation (or thresholding) in matrix D . Thus Eq. 8 is updated as:

$$T_{trunc}^{-1} = V \cdot D_{trunc}^{-1} \cdot U^T \quad (9)$$

We refer the reader to the work of Redding *et al.* [8] for a detailed explanation of the spectrum reconstruction.

V. EXPERIMENTAL SETUP

The experimental setup was already illustrated in Figure 1, to clarify the proposed architecture. We utilize a tunable laser source (Sacher Lasertechnik /TEC-500-0850-030-M) for calibration and a fiber coupled super luminescent diode – (Inphenix/IPSDD0815) to perform reconstruction. Without loss of generality, we utilize cylindrical lens having focal lengths of 70 mm, 80 mm, and 100 mm for focusing on the scatterer, collimation, and re-focusing on the CCD camera. Note that the usage of the last focusing lens results in relatively small speckle spots (~ 3 camera pixels wide) ensuring significant change of the speckle pattern with wavelength shift. Bigger speckle spots would result in a very limited number of speckle spots and thus significantly hamper the performance of the SEPS device.

The utilized setup maps the monochromatic source to a vertical line. Based on Eq. 1, we calculate the theoretical FWHM prism resolution (without the scatterer) as $\Delta\lambda_{prism} \sim 1.587$ nm for experimental conditions ($\sigma' = 0.42 \times 10^{-4}^\circ / \text{nm}$, $W = 5$ mm, $\lambda = 855$ nm). The prism resolution is measured

TABLE I
RESOLUTION AND DYNAMIC RANGE ACHIEVED
WITH EXPERIMENTED SCATTERERS

	Resolution (pm) ($\Delta\lambda_{SEPS}$)	Resolution (K)	Gain	Dynamic Range (DR)
No scatterer	1680	1		450
Grinded glass	526	3.19		1,438
Adhesive tape	373.8	4.49		2,023
Sketch paper	201.7	8.32		3,750
Parchment	200.2	8.39		3,778
TiO ₂ mixture 1	39.4	42.63		19,200
TiO ₂ mixture 2	30	56		25,217
TiO ₂ mixture 3	17.1	98.24		44,240

as 1.68 nm through i) observing the pixel shift on the CCD camera due to a given wavelength shift and then ii) observing the FWHM width of the captured line for a single wavelength. Based on the wavelength / pixel count of 0.54 pixels / nm, The CCD camera, having 1392 horizontal pixels maps to a wavelength range ($\Delta\Lambda$) of 756.5 nm, matching the wavelength range (350 - 1100 nm) of which can be detected by a silicon based detector. Thus the dynamic range (D.R) of SEPS could be expressed as:

$$D.R = \frac{\Delta\Lambda}{\Delta\lambda_{SEPS}} = K \cdot \frac{\Delta\Lambda}{\Delta\lambda_{prism}} \quad (10)$$

Despite the presence of the slit, placed right after the scatterer, the line width per wavelength observed on the detector varies based on the scatterer type, as the scatterer acts as a numerical aperture expander as well. The overall observed line width sets the wavelength range to calculate the spectral correlation: $C(\Delta\lambda, x)$, below which cannot be resolved by the prism spectrometer alone.

The scattering layer is the heart of the proposed spectrometer device. We utilize a variety of scatterers, including nanoparticle – epoxy mixtures that can be precision tailored via altering mixture ratio, and single side grinded microscope slides. We also utilize practical low-cost tools such as parchment paper, sketch paper and adhesive tape as scatterers. The nanoparticle-based scatterers were prepared through mixing TiO₂ nanoparticles: ultraviolet (UV) curable epoxy mixture with various mass ratios. Two thin cylindrical rod spacers with desired thicknesses are placed in between two glass slides to maintain the desired thickness. Then, the prepared mixture is drained between the two slides, minimizing entrapping of air bubbles and allowing for a more controlled scatterer production. The sandwiched mixture is finally UV and heat cured. Note that, other scatterers require minimal or no preparation.

VI. RESULTS

The system performance was first demonstrated through conducting a series of calibration routines (with 10 pm wavelength steps), and calculating the spectral correlation function. Table 1 summarizes the resolution and dynamic range achieved using all tested scatterers. Three nanoparticle epoxy mixtures were prepared where mixture 1 was prepared having 750 μm thickness, and 1:25 TiO₂-to-epoxy mass ratio, mixture 2 with 400 μm thickness, and 1:12 TiO₂-to-epoxy mass ratio, and finally mixture 3 with 750 μm thickness,

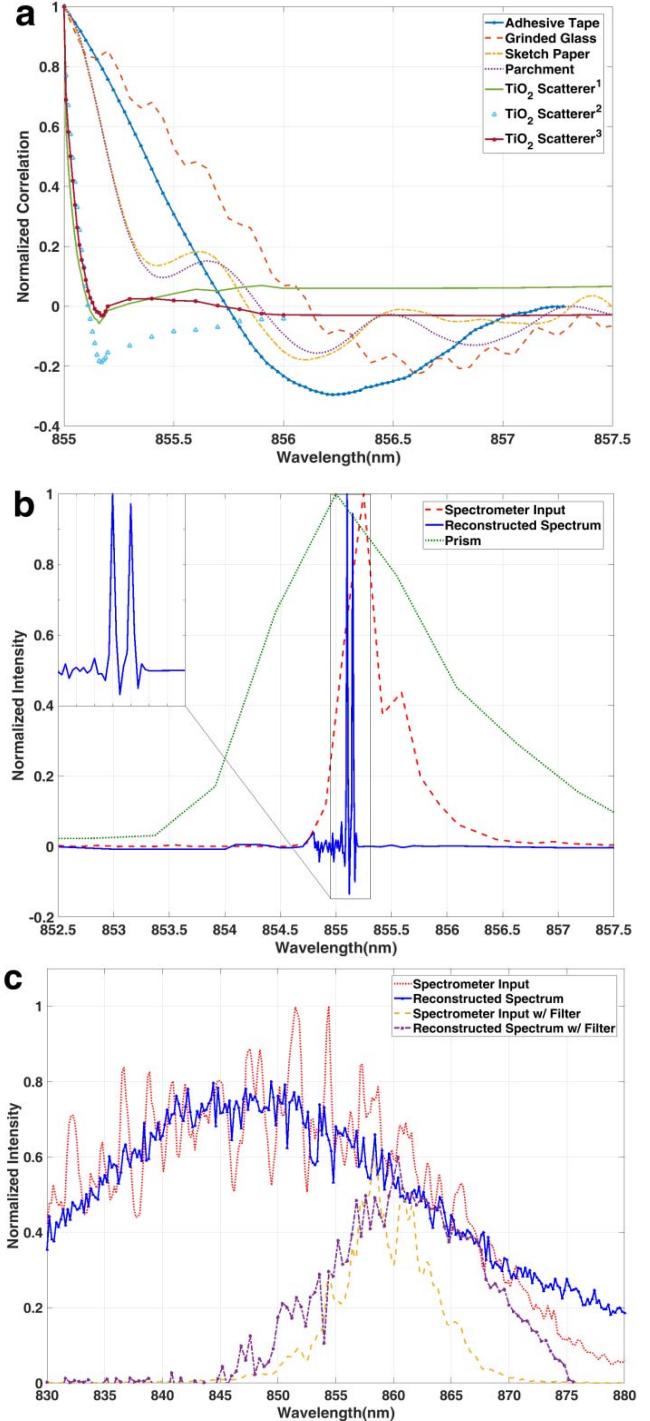


Fig. 2. Characterization of the SEPS device with nanoparticle mixture scatterer; a) spectral correlation b) reconstruction of two added speckle patterns for $\lambda_1 = 855.1\text{nm}$ and $\lambda_2 = 855.15\text{ nm}$, c) reconstruction obtained for SLD input (with and without bandpass filter).

and 1:12 TiO₂-to-epoxy mass ratio. Mixture 3 achieved the best resolution of 17 pm (mixture 3), while mixture 1 and 2 showcased a correlation of 39.4 pm and 30 pm, respectively. Though the light budget of our system can handle higher mixture concentrations, the minimum wavelength step of the tunable laser limited our ability to measure a narrower correlation. Thus we report the best resolution above the minimum wavelength step, (17 pm, resolution that was observed with

interpolation of the correlation plot that is near twice wider than the wavelength step). The parchment and sketch paper provided ~ 200 pm resolution and the adhesive tape could only provide a resolution of 373.8 pm. Finally the grinded glass provided ~ 520 pm resolution. Note that the acquired resolution values are representative, and may change upon using different brands (for parchment & sketch paper and adhesive tape) or applying different grade grinders and duration on the glass. Note that the monotonically decreasing nature of the spectral correlation function (apart from the fluctuations around zero correlation value) is an indicator that the speckle patterns are unique within the acquired range.

We now concentrate on the best performing scatterer, the nanoparticle mixture 3, to perform reconstruction of i) digitally added speckle patterns of two wavelengths (where additional speckle images were acquired besides the calibration images) placed 50 pm apart and ii) the SLD source with and without a 12-nm FWHM bandpass filter. Figure 2 illustrates the spectral correlations for all scatterers, two wavelength reconstruction, and broad-band reconstruction performance of the SEPS system employed with the nanoparticle mixture 3 scatterer. The results showcased in Fig 2b,c are escorted with the results obtained with a commercial grating spectrometer (Thorlabs / CCS175/M), having 400 pm spectral resolution. The commercial spectrometer falls short in resolving two separate but close wavelengths; the SEPS clearly shows two clearly distinguished peaks. Table 1 suggests that the peaks could have been resolved with other nanoparticle mixtures as well. We attribute the discrepancy between SEPS and the commercial grating spectrometer results to the diminished optical power of our tunable laser source between 870–880 nm wavelengths, which leads to the reconstruction error at this particular spectral range. Furthermore, non-optimal selection of the threshold in Eq. 9, and limited area selection of the speckle patterns (as opposed to using the entire image) due to memory limitation of the utilized computer are yet other potential sources of reconstruction error.

VII. CONCLUSIONS AND DISCUSSION

In this work, we've introduced the speckle-enhanced prism spectrometer, with which we demonstrated up to a spectral resolution of 17 pm, revealing a wide dynamic range of $\sim 44,500$. This spectrometer architecture is particularly appealing owing to its simple setup, only necessitating a simple add-on to the conventional prism spectrometer. Through utilizing a higher sensitivity, lower noise camera in conjunction with a highly scattering layer, it would indeed be possible to improve the obtained dynamic range.

Practical realization of the proposed SEPS device would require the scattering layer to be placed on a closed-loop

temperature and humidity controller, the use of athermal optomechanics, precise control of the light source for low-noise operation, to eliminate any drifts in alignment resulting in deviations of the speckle patterns. Calibration is only required once per scatterer, and the acquired speckles could be utilized to measure multiple sources and any material under test that is introduced within the spectrometer path. Furthermore, optical throughput of the device is yet another important aspect for practical purposes. Empirically, we've observed direct proportionality between optical throughput and the resolution. Thus, highly scattering layers offer a high-dynamic range at the expense of high detector exposure, which would hamper real-time realization. One solution to the optical throughput problem is to utilize scattering waveguides that could achieve near unity throughput while still offering good spectral resolution. As a future work, we aim to i) conduct a thorough study on a variety of scatterers to reveal the relation between mixture attributes and the resultant spectral correlation width, and ii) integrate the SEPS into a Fourier-Domain Optical Coherence Tomography (OCT) imager to uncover deep tissue layers.

REFERENCES

- [1] B. Meyer and T. Peters, "NMR spectroscopy techniques for screening and identifying ligand binding to protein receptors," *Angew. Chem.-Int. Ed.*, vol. 42, no. 8, pp. 864–890, 2003.
- [2] O. Beyssac, B. Goffé, J.-P. Petitet, E. Froigneux, M. Moreau, and J. N. Rouzaud, "On the characterization of disordered and heterogeneous carbonaceous materials by Raman spectroscopy," *Spectrochimica Acta A, Mol. Biomol. Spectrosc.*, vol. 59, no. 10, pp. 2267–2276, 2003.
- [3] M. Jöhnck, L. Müller, A. Neyer, and J. W. Hofstraat, "Copolymers of halogenated acrylates and methacrylates for the application in optical telecommunication: Optical properties, thermal analysis and determination of unsaturation by quantitative FT-Raman and FT-IR spectroscopy," *Eur. Polym. J.*, vol. 36, no. 6, pp. 1251–1264, 2000.
- [4] R. Leitgeb, M. Wojtkowski, A. Kowalczyk, C. K. Hitzenberger, M. Sticker, and A. F. Fercher, "Spectral measurement of absorption by spectroscopic frequency-domain optical coherence tomography," *Opt. Lett.*, vol. 25, no. 11, pp. 820–822, 2000.
- [5] H. W. Siesler, Y. Ozaki, and S. Kawata, *Near-Infrared Spectroscopy. Principles, Instruments, Applications*, vol. 16, no. 12. Weinheim, Germany: Wiley, 2002.
- [6] S. H. Kong, D. D. L. Wijngaards, and R. F. Wolffenbuttel, "Infrared micro-spectrometer based on a diffraction grating," *Sens. Actuators A, Phys.*, vol. 92, nos. 1–3, pp. 88–95, 2001.
- [7] B. Redding, M. Alam, M. Seifert, and H. Cao, "High-resolution and broadband all-fiber spectrometers," *Optica*, vol. 1, no. 3, pp. 175–180, 2014.
- [8] B. Redding, S. M. Popoff, and H. Cao, "All-fiber spectrometer based on speckle pattern reconstruction," *Opt. Express*, vol. 21, no. 5, pp. 6584–6600, 2013.
- [9] N. H. Wan, F. Meng, T. Schröder, R.-J. Shiue, E. H. Chen, and D. Englund, "High-resolution optical spectroscopy using multimode interference in a compact tapered fibre," *Nature Commun.*, vol. 6, Jul. 2015, Art. no. 7762.
- [10] E. Hecht, *Optics*, vol. 1, 4th ed. Reading, MA, USA: Addison Wesley, 2001, p. 122.
- [11] J. C. A. Barata and M. S. Hussein, "The Moore–Penrose pseudoinverse: A tutorial review of the theory," *Brazilian J. Phys.*, vol. 42, nos. 1–2, pp. 146–165, 2012.